24th COBEM - 2017

24th ABCM International Congress of Mechanical Engineering
December 3-8, 2017, Curitiba, PR, Brazil

COBEM-2017-1454
INFLUENCE OF HYDRATE-LIKE SOLID PARTICLES IN HORIZONTAL GAS-LIQUID SLUG FLOWS

Rafael F. Alves
Luis M. M. Rosas
Carlos L. Bassani
Fábio A. Schneider
Marco J. da Silva
Moisés A. Marcelino Neto
Rigoberto E. M. Morales
Multiphase Flow Research Center (NUEM), Federal University of Technology – Paraná (UTFPR). Rua Deputado Heitor Alencar Furtado 5000, Bloco N, CEP 81280-340, Curitiba, Brazil
rmorales@utfpr.edu.br

Amadeu K. Sum
Hydrates Energy Innovation Laboratory, Chemical and Biological Engineering Department, Colorado School of Mines, 1500 Illinois St., CO 80401, Golden, USA.

Abstract. *Gas hydrate formation is a main flow assurance concern in oil and gas production due to the high risk of flow disruption and possible blockages. One of the major knowledge gap in the strategy for hydrate management is the impact of hydrates on the multiphase flow, as hydrates are solid particles that may be dispersed in the liquid and transported as a slurry. While there is anecdotal evidence for the influence of hydrates on the flow hydrodynamics, no studies have fundamentally addressed this topic. For offshore operations, the phases are assumed as flowing predominantly in the slug flow pattern due to the range of gas and liquid superficial velocities. Understanding the effects of the introduction of solid particles in the slug flow is essential to improve the efficiency and safety of multiphase production. The purpose of the present work is to experimentally characterize solid-liquid-gas slug flow with the presence of homogeneously dispersed hydrate-like particles. Experimental tests were carried out with inert polyethylene particles of 0.5-mm diameter with density similar to gas hydrates (938 kg/m3). The test section comprised a 26-mm ID, 9-m length horizontal duct made of transparent Plexiglas. High Speed Imaging was used to analyze the slug flow unit cell behavior due to the introduction of the solid particles. Two distinct concentrations of solid particles were tested (6 and 8 g/dm3) and compared to a similar case of liquid-gas slug flow.*

Keywords: *flow assurance, hydrates, three-phase, solid-liquid-gas, slug flow.*

1. INTRODUCTION

The slug flow pattern is the prevailing flow regime in offshore oil and gas production due to the characteristic operational conditions. Slug flow is characterized by the intermittent succession of two structures: (i) a liquid slug, which may or may not contain dispersed gas bubbles in it, and (ii) an elongated bubble sliding over a thin liquid film. Together, those two structures constitute that what is known as a slug flow unit cell (Wallis, 1969). The slug and the elongated bubble possess characteristic velocities and geometric features such as lengths and phase fractions. Those characteristics depend on time and space and their prediction is relevant in the design of offshore production systems.

Besides oil and gas, offshore operations may also contain water (brine) and solid particles dispersed in the mixture, such as sand. Furthermore, water and gas at high pressure and low temperature conditions – often found in offshore production – favor the formation of gas hydrates. Gas hydrates are crystals formed by the trapping of gas molecules into cages formed by hydrogen-bonded water molecules (Sloan and Koh, 2008) and are a major concern due to the potential blockage risks of flowlines, with consequent economic losses and safety concerns caused by production interruption. Hydrates can form at the gas-water interface, where a more effective contact between the phases occurs (Sloan *et al*., 2011), thus forming a dispersion. The dispersion may be homogeneous or heterogeneous, depending on the concentration and size of the particles (Peker and Helvaci, 2007). At some point, the particles may agglomerate due to

capillary and intermolecular forces (Camargo *et al*., 2000), forming: (i) a moving or stationary bed, causing a restriction in the flow cross sectional area; or (ii) a massive plug, which will stop production.

Pipe blockage due to hydrate formation is one of the main challenges faced by oil and gas production companies, especially when dealing with deep and cold waters (Cardoso *et al*., 2015). Efforts have been made on experimentally characterizing and modeling gas-liquid slug flow (Bassani *et al*., 2016; Castillo, 2013; França *et al*., 2008; Issa and Kempf, 2003; Kjeldby *et al*., 2013; Rogero, 2009; Shoham, 2006; Taitel and Barnea, 1990) and solid-liquid flow (Crowe *et al*., 2012; Doron *et al*., 1987; Doron and Barnea, 1993; Gore and Crowe, 1989; Guer *et al*., 2003; Kaushal *et al*., 2005; Kaushal and Tomita, 2002). However, studies on three-phase solid-liquid-gas flow are scarce and focused in the flow effects on the transportation of the solid particles (Dabirian *et al*., 2016a, 2016b; Goharzadeh *et al*., 2010; Goharzadeh and Rodgers, 2009; Orell, 2007; Stevenson *et al*., 2001; Stevenson and Thorpe, 2003, 2002), but do not comprise the effects of the particles in the flow hydrodynamic characteristics, such as the slug flow frequency, the unit cell translational velocity and the geometry of the unit cell structures. The majority of the literature studies also assume particles with density much higher than water, such as sand. However, this is not the case of gas hydrates, which are slightly lighter/heavier than water/oil and thus tending to easily flow with the carrying liquid.

The present study aims to experimentally characterize three-phase solid-liquid-gas (polyethylene-water-air) slug flows in horizontal pipes. The slug flow pattern was chosen since it is the prevailing one in offshore oil operations. To avoid experimentation with real hydrate particles – which would demand a high pressure flowloop, with a precise temperature and pressure monitoring system – inert polyethylene particles were chosen to represent the hydrates having similar density and size (938 kg/m3 with 0.5 mm diameter). This study is the first attempt, to the best of our knowledge, to understand the influence of hydrate-like solid particles on the main parameters of the slug flow by means of High Speed Imaging.

2. EXPERIMENTAL FLOWLOOP

An experimental flowloop was assembled to characterize three-phase solid-liquid-gas horizontal slug flows using High Speed Imaging. Table 1 presents the experimental flowloop characteristics and the range of parameters covered during the measurements. The fluids used were air and water at ambient conditions (approximately 100 kPa and 298 K). A total of 9 liquid-gas superficial velocities combinations were measured for two different solid particles concentration (6 and 8 g/dm^3). Two-phase liquid-gas flow – that is, without the solid particles (indicated as 0 g/dm^3) – was also measured at the same conditions for comparison purposes. Each measurement was made three times to assure repeatability. Figure 1 presents the pairs of liquid and gas superficial velocities plotted inside the flow map of Taitel and Dukler (1976). All the measurements fall within the slug flow pattern, the exception for j_L = 0.75 m/s and j_G = 0.25 m/s, which is a case of plug flow – a subcase of intermittent flow that presents different morphologies of the elongated bubble nose and tail (Thaker and Banerjee, 2016). Since this case presented similar trends with the others, it will therefore be analyzed together with them.

Table 1. Experimental flowloop characteristics and range of measured parameters.

Fluids	Air and water, at slug flow pattern
Particles material/density/diameter	Polyethylene / 938 kg/m^3 / 0.5 mm
Pipe wall material	Plexiglas, transparent
Pipeline inclination/ID	Horizontal / 26 mm
Flowloop total length	9 m (~346 ID)
Measurement station position	6.45 m (~248 ID)
Flowloop pressurization	Ambient
Flowloop temperature	Ambient, isothermal
Liquid superficial velocity range	$0.25 \leq j_L \leq 1.5$ m/s
Gas superficial velocity range	$0.25 \leq j_G \leq 1.5$ m/s
Solid particles concentration	0 / 6 / 8 g/dm^3
Mixture superficial velocity range	$1 \leq J \leq 2$ m/s

Figure 2 shows a schematic of the experimental flowloop. Water is stored in a tank (i) of 250 dm^3, where the solid particles are added at the desired concentration. A mixer (ii) is placed inside the tank to assure a homogeneous dispersion. The solid-liquid dispersion passes through a centrifugal pump (iii) for up to 200 kPa, which is fed by a 3 hp electric motor (iv). The water flow rate is controlled by a variable-frequency drive (v) actuating on the electric motor. A Coriolis-type flowmeter (vi) is positioned downstream of the pump and upstream of the mixing location with the gas phase. The Coriolis returns the density and mass flow rate of the solid-liquid dispersion.

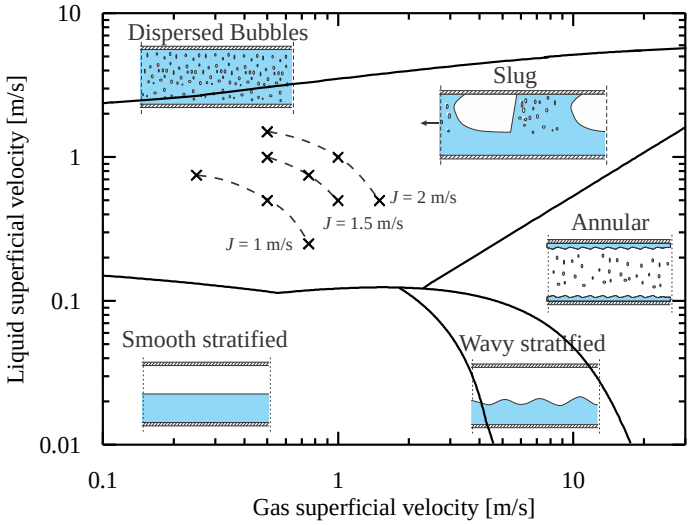

Figure 1. Pairs of superficial velocities inside of the gas-liquid two-phase flow map of Taitel and Dukler (1976). Air-water, 26-mm ID horizontal pipe.

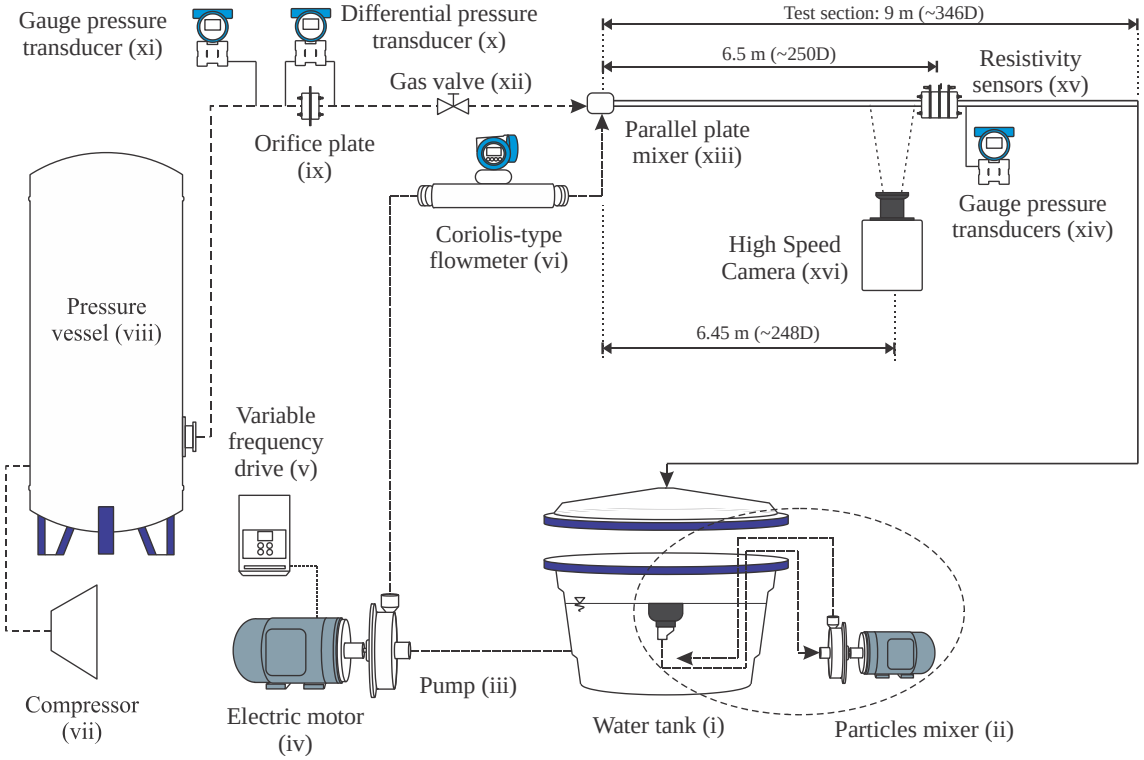

Figure 2. Schematic diagram of the experimental flowloop used for the characterization of three-phase solid-liquid-gas flow.

In a parallel branch of the flowloop, air is compressed (vii) up to 800 kPa. The air is stored in two pressure vessels (viii) with working pressure of 1.4 MPa and combined capacity of 600 dm^3. The gas flow rate is measured through an orifice plate (ix). A differential pressure transducer (x), designed for a measurement range of 0 to 60 kPa, evaluates the pressure drop in the orifice plate. The pressure difference is correlated to the volumetric flow rate via calibration with a rotameter, with a maximum deviation of ±2.9%. Additionally, the gas density is evaluated using empirical correlations (Fox et al., 2011) as a function of the local air temperature and gauge pressure (xi) measured at the orifice plate inlet. The gas flow rate is controlled by a manual valve (xii) positioned downstream of the orifice plate.

The phases are mixed at the inlet of the horizontal pipeline via a parallel plate mixer (xiii), which locally generates a stratified flow pattern. This pattern should naturally evolve to slug flow if the superficial velocities of the phases are propitious, which was indeed the case for all the liquid-gas superficial velocity combinations measured in this study. In order to ensure this flow pattern transition, the High Speed Camera (xvi) was positioned at 6.45 m (~248 ID) from the

pipe inlet. A gauge pressure transducer (xiv) is inserted next to the Camera. The total length of the flowloop is approximately 9 m (~346 ID), thus assuring approximately 2.55 m (~98 ID) of pipeline before the return bend to the water tank, avoiding any reverse upstream effects. The fluids are then discharged back to the water tank, where the separation of the phases occurs naturally by gravity. The air is released to the ambient, while the solid-liquid dispersion is reinjected on the flowloop.

The High Speed Camera is used to visualize the flow pattern. The acquisition rate can be set for up to 3600 frames per sec at its higher resolution of 1024×1024 pixels. To avoid light refraction, a box made of Plexiglas filled with water was positioned so as to wrap the pipe. A light source with a diffuser surface was used to enhance image contrast.

A pressure transducer is positioned near the resistivity sensor to estimate the local gas superficial velocity, which is accomplished by comparing the pressures at the test section inlet and at the orifice plate. Using the volumetric gas flow rate measured by the orifice plate $\dot{Q}_{G,orifice\ plate}$ and dividing by the cross-sectional area of the pipe:

$$j_{G,test\ section} = \frac{P_{orifice\ plate}}{P_{test\ section}} \frac{4\dot{Q}_{G,orifice\ plate}}{\pi D^2} \tag{1}$$

The Coriolis measures the particles-in-water dispersion mass flow rate and its density. Therefore, the dispersion superficial velocity is calculated as:

$$\tilde{j}_L = \frac{4}{\pi D^2} \frac{\dot{m}_{Coriolis}}{\rho_{Coriolis}} \tag{2}$$

where the notation $(\tilde{\bullet})_L$ stands for the dispersion. The liquid superficial velocity is therefore calculated in terms of the amount of particles inserted in the water tank as:

$$j_L = \frac{4}{\pi D^2} \frac{\dot{m}_{Coriolis}}{\rho_{Coriolis}} \left(1 + \frac{m_S}{\rho_S V_{L,tank}} \right)^{-1} \tag{3}$$

where m_S is the mass of solid particles inserted at the water tank with volumetric capacity of $V_{L,tank}$ and ρ_S is the density of the particles.

A computer registers the signals coming from the flowmeter, the orifice plate (that is, the calibrated pressure transducer) and the test section pressure transducer. The High Speed Imaging data are registered in a storage drive inside the camera. The gas and liquid superficial velocities are calculated via Eqs. (1) and (3), respectively, and controlled during the tests to do not fluctuate more than ±1% around the nominal values of Table 1. Some minor fluctuations are, however, intrinsic of the slug flow pattern.

3. THEORY ON THE EFFECTS OF PARTICLES IN GAS-LIQUID FLOW

Before discussing the analysis of the results, it is interesting to discuss the main effects brought by the introduction of the solid particles in the flow. These effects can be divided into:

(A) Properties variation: the homogeneous particle-in-water dispersion can be treated as a liquid phase with equivalent properties. That is, the three-phase solid-liquid-gas flow can be regarded as a pseudo two-phase flow of dispersion and gas. The dispersion equivalent properties are dependent on the particles volumetric fraction inside the liquid, calculated as $R_{S/L} = m_S / (\rho_S V_{L,tank})$ (non-slip assumption). The volumetric fraction stays in the range of $0 \le R_{S/L} \le 0.0085$ for the evaluated cases.

The dispersion density can be calculated via an homogeneous model (Shoham, 2006) as $\tilde{\rho}_L = \rho_S R_{S/L} + \rho_L (1 - R_{S/L})$. For the cases when $R_{S/L} = 0.0085$, the density of the dispersion is approximately 0.05% smaller than the density of the liquid, a negligible change.

The dispersion viscosity (in laminar regime) can be estimated by the Krieger and Dougherty's (1959) correlation for spherical particles with maximum package factor of 0.63, $\tilde{\mu}_L = \mu_L (1 - R_{S/L}/0.63)^{-1.575}$. For the cases when $R_{S/L} = 0.0085$, the dispersion viscosity is approximately 2.2% higher than the water viscosity. It is important to notice that the turbulent viscosity will depend on the turbulent intensity in each part of the unit cell (film, slug, wake of the elongated bubble) and on the turbulence modulation due to the particles introduction – to be discussed.

Finally, if the solid particles reach the liquid-gas interface, they may curve it. Therefore, a stress of the interface may occur, increasing the amount of energy distributed in the surface [J/m^2]. Since this is the thermodynamic definition for interfacial tension, then the presence of the solid particles may increase the interfacial tension between the gas and the liquid, thus changing the behavior between the bubbles, such as their coalescence rate. Measurements for evaluating the variation in the interfacial tension due to the solid particles introduction are required in future analysis.

(B) Turbulence modulation by particles: in (A), the phenomenon is treated as pseudo two-phase flow between the dispersion and the gas. However, this approach does not capture the interaction between the solid particles and the liquid flow. The presence of the particles can either damp or promote turbulence (Gore and Crowe, 1989). Small particles (compared to the length of the most energetic eddy) will follow the eddy for at least part of its lifetime, therefore consuming the energy of the eddy and decreasing the turbulence intensity. By its turn, larger particles do not follow the eddy and promote turbulence due to the relative motion between the particle and the fluid, which may create local vortexes.

Gore and Crowe (1989) propose a criterion to understand when the presence of particles increase or decrease the turbulence intensity based on the ratio between the particle diameter and the most energetic length, d_P/ℓ_e. They found that experimental data for a wide range of parameters behave well for a criterion of $d_P/\ell_e\big|_{crit} \approx 0.1$. Hutchinson *et al*. (apud Gore and Crowe, 1989) showed that the most energetic eddy presents an approximately constant length of 20% of the pipe radius (not valid for regions near the wall). Since $d_P/\ell_e \approx 0.2$ for the present case of study, then the particles are most prone to promote turbulence on the liquid phase.

(C) Mixture superficial velocity variation: in order to have a direct comparison between the two-phase liquid-gas and the three-phase solid-liquid-gas flows – to understand the influence of the introduction of the particles – the experimental data need to present isonomy. That is, everything else other than the introduction of the particles should be kept as constant as possible to isolate the effects of the solid phase.

The fixed parameters during the measurements are the liquid (j_L) and the gas (j_G) superficial velocities. However, the presence of a slurry flow is associated to the insertion of a solid superficial velocity (j_S). Shoham (2006) shows that, for an ideal case of non-slip flow, the volumetric fraction of the particles inside the liquid can be estimated as the ratio between the solid and the liquid superficial velocities, $R_{S/L} = j_S/j_L$. This is a reasonable assumption for homogeneous solid-liquid flows and for small differences between the densities of the phases, which is indeed the case of the present study. Upon isolating the solid superficial velocity, it can be written as $j_S = R_{S/L} j_L$. Shoham (2006) also affirms that the mixture superficial velocity is the sum of the superficial velocities of all the phases, $J = j_L + j_G + j_S$. Since the gas and liquid superficial velocities remains constant, but the solid concentration changes, then the mixture superficial velocity increases in $\Delta J \approx j_S = R_{S/L} j_L$ with the particles introduction.

The maximum mixture velocity variation due to the introduction of the particles in the case of study is $\Delta J_{\max} \approx 0.013 m/s$. This variation is under the uncertainties of the experiments, related to up to 0.035 m/s of variation in the mixture superficial velocity. Therefore, even if the introduction of the solid particles may cause a little acceleration of the flow, the experimental apparatus is not prepared to capture it, and therefore the experiments can be considered in conditions of isonomy.

The results will be discussed next in means of the aforementioned effects brought by particles introduction in the gas-liquid slug flow.

4. SLUG FLOW VISUALIZATION

The images from the camera allow a qualitatively discussion of the morphology of the slug flow structures, presenting phenomena either that are intrinsic of two-phase gas-liquid flows (which keep occurring in three-phase flow) or due to the introduction of the solid particles. Next, those discussions are made for the following regions of the unit cell: the elongated bubble nose, the film and the slug body (specially focusing on the elongated bubble wake). The images showed are representative of the entire data set measured.

4.1 Elongated bubble nose

Figure 3 presents three different elongated bubble noses for each particle concentration (0, 6 and 8 g/dm^3), maintaining the gas and superficial velocities at $j_L = j_G = 1$ m/s. Following Taitel and Barnea's (1990) theory, the introduction of the solid particles – which cause the relative properties of the dispersion to change, effect (A) – should change the elongated bubble shape. The authors model the elongated bubble profile in terms of a combined gas-liquid momentum balance, and therefore properties variation should change the value of the inertial and shear stress terms, thus causing the bubble profile to change. Mazza *et al*. (2010) affirm that higher liquid viscosities are related to thinner elongated bubbles. Furthermore, the shear stress terms could also be changed by turbulence modulation – effect (B).

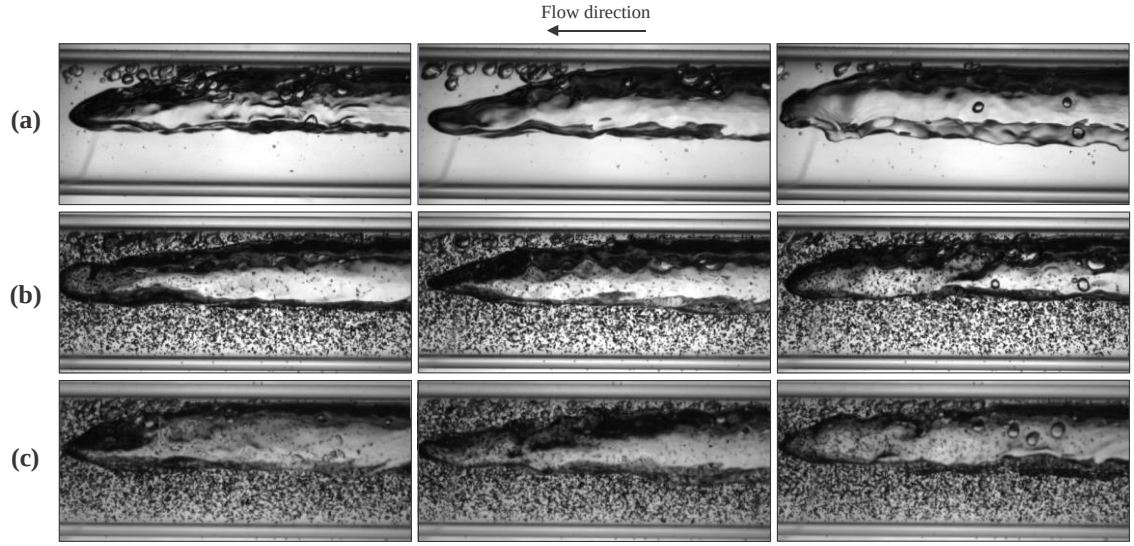

Figure 3. Elongated bubble nose for the following particles concentration: (a) 0 g/dm^3, (b) 6 g/dm^3 and (c) 8 g/dm^3 ($j_L = j_G = 1$ m/s).

However, it can be seen that the profile of the elongated bubble nose (Figure 3) changes from bubble to bubble even if the same conditions are maintained (same particle concentration and gas and liquid superficial velocities), which is due to the slug flow intermittent nature. To understand if the particles introduction in the experiments is sufficient to cause perceptive variations in the elongated bubble nose, its profile need to be somehow measured quantitatively. For this purpose, a ruler was positioned near the pipe wall. Knowing the pipeline inner diameter, the *x-y* coordinates of the bubble profile were mapped using the software Web Plot Digitizer (Rohatgi, 2010).

Analyzing the bubble profiles, it is clear that the intermittence of the flow – that is, the variations on the profile from bubble to bubble maintaining the same conditions of solid particles – are higher than the variations due to the introduction of the solid particles for the experiments done. That is, no perceptive variation on the bubble nose profile was found in the present data due to the presence of the solid particles.

4.2 Slug region andelongated bubble wake

Figure 4 shows an assembly of images along the slug region for each particle concentration and for $j_L = j_G = 1$ m/s. The dispersed bubbles released in the slug body tend to follow the elongated bubble if inside the wake zone (number 1). The dispersed bubbles present some oscillations in this region due to the presence of high recirculation intensity. Once 'escaping' this recirculation zone, the buoyance forces predominate and the dispersed bubbles migrate to the upper wall (number 2). The liquid velocity in the upper wall is lower than in the centerline of the slug, and therefore the dispersed bubbles are slowly left behind until reaching the next elongated bubble nose (number 3). The smaller dispersed bubbles remain stable at the centerline of the slug, since the buoyance forces are not sufficient to overcome the turbulent forces when the bubble diameter is sufficiently small (number 4).

When introducing the solid particles (Figure 4(b) and (c)), a higher amount of dispersed bubbles seems to be present at the slug body (number 5). The visualization of the slug region with the presence of the solid particles is however disturbed, since both particles and gas dispersed bubbles tend to darken the image. The release of dispersed bubbles in the slug body also depends on the intermittence of the slug flow, and therefore Figure 5 presents three different wake zones of the elongated bubble for each particle concentration. It is qualitatively perceptible that the amount of dispersed bubbles released in the slug body is higher for the cases with solid particles in the analyzed images. However, a quantitative analysis is needed to evaluate the population and the size of the dispersed bubbles in function of the presence of the solid particles.

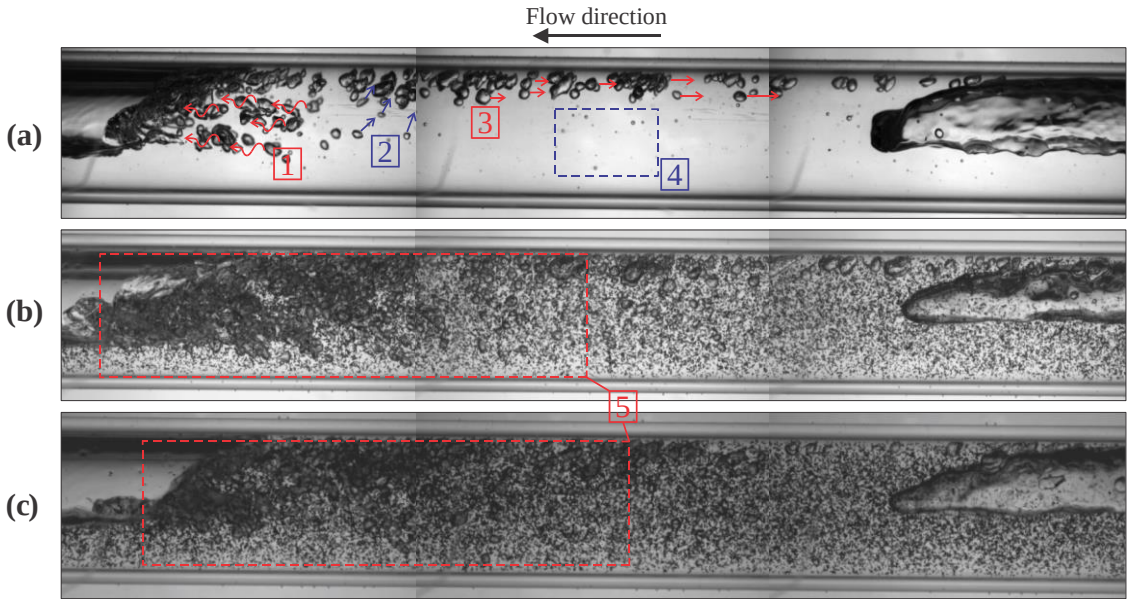

Figure 4. Slug region for the following particles concentration: (a) 0 g/dm^3, (b) 6 g/dm^3 and (c) 8 g/dm^3 (j_L = j_G = 1 m/s).

Figure 6 shows the bubble wake zone with schematics for the phenomena involved. The gas dispersed bubbles are released in the slug body due to the shear stress caused by the recirculation zone (number 2). When inside this recirculation zone, the dispersed bubbles follow the elongated bubble tail (number 3). The nearest dispersed bubbles from the elongated bubble tail tend to recoalesce with the elongated bubble (number 1), while the farther tend to 'escape' the recirculation zone, where the buoyance forces are dominant and then cause the dispersed bubbles to migrate to the upper wall (number 4).

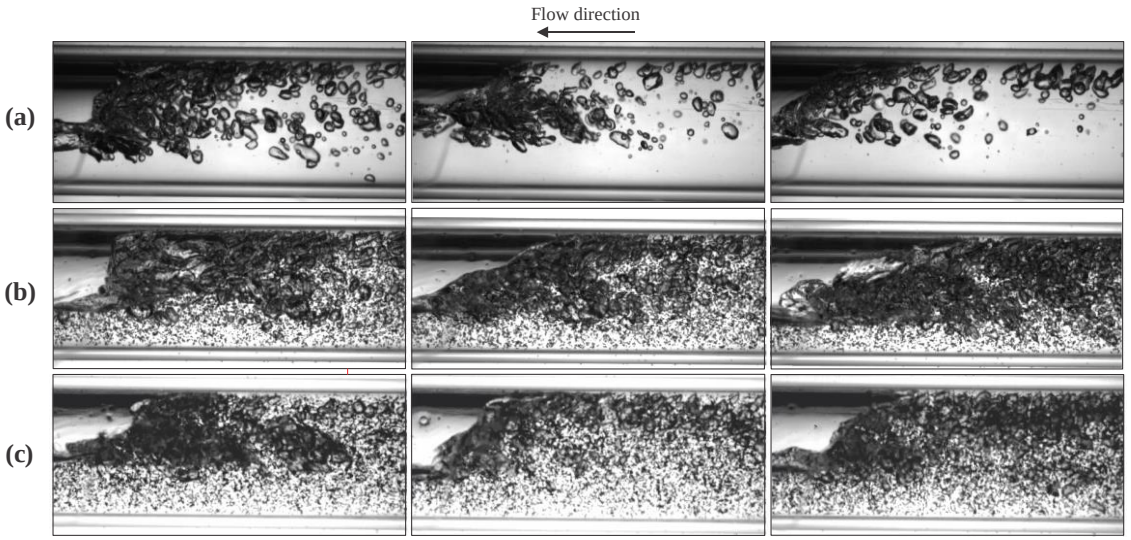

Figure 5. Elongated bubble wake for the following particles concentration: (a) 0 g/dm^3, (b) 6 g/dm^3 and (c) 8 g/dm^3 (j_L = j_G = 1 m/s).

Figure 7 shows evidence of the recoalescence of a dispersed bubble with the elongated bubble tail. Figure 7(a) and (b) show the dispersed bubble approaching the elongated bubble tail and in Figure 7(c) the recoalescence process starts. In Figure 7(d), the interface between the dispersed bubble and the elongated bubble is not clear anymore, and the mass transfer process begins. The dispersed bubble mass is rapidly incorporated to the elongated bubble. Figure 7(e) shows the elongated bubble rear right after the end of the recoalescence process.

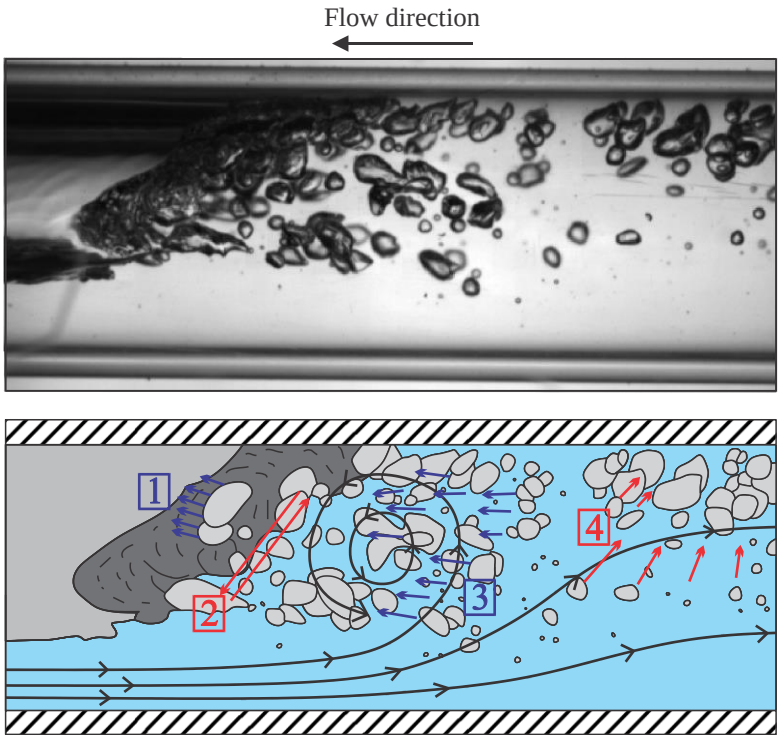

Figure 6. Close in the elongated bubble wake, with schematics of the involved phenomena (j_L = j_G = 1 m/s). Liquid streamlines are relative to the elongated bubble motion.

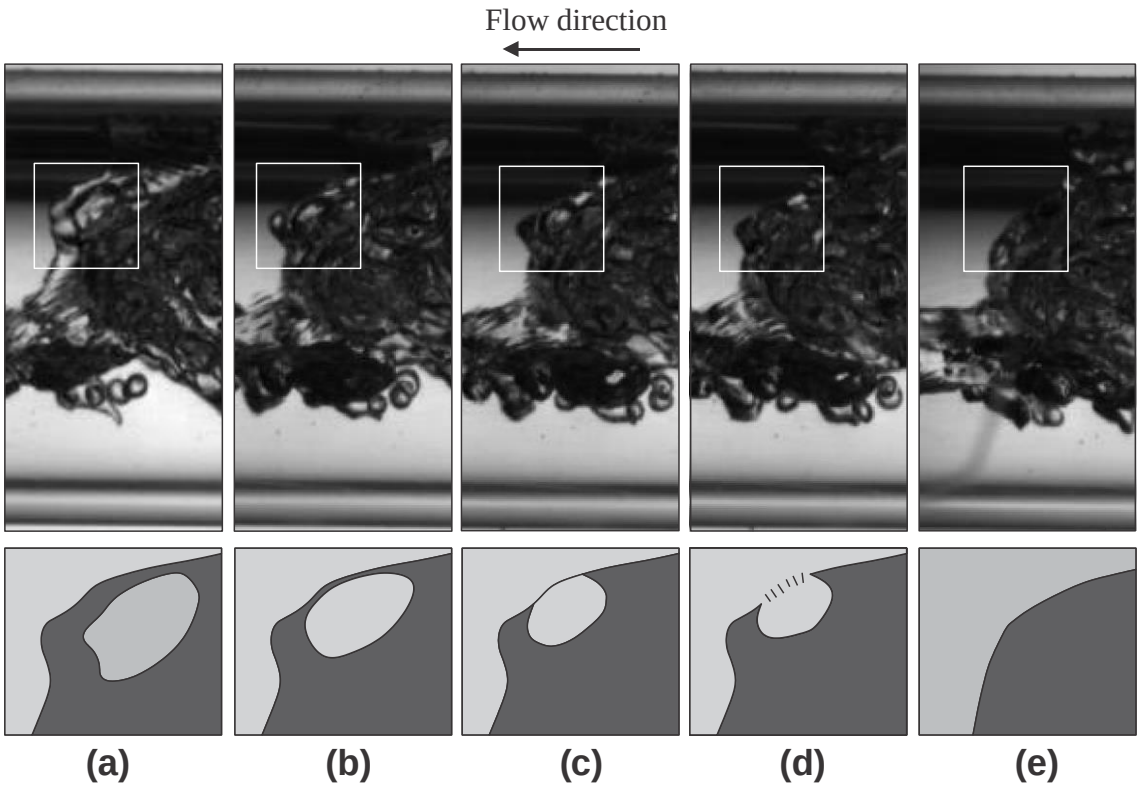

Figure 7. Dispersed bubble recoalescing with the elongated bubble rear (j_L = j_G = 1 m/s. (a) Dispersed bubble approaching the elongated bubble rear, (b) recoalescence in the imminence of starting, (c) recoalescence starts, (d) interface vanishes and (e) recoalescence ends.

The amount of gas dispersed in the slug body, R_{GS}, will therefore be proportional to the difference in the rate of dispersed bubbles released by the elongated bubble tail, $\dot{q}_{release}$, and to rate of dispersed bubbles that recoalesce with the elongated bubble tail, $\dot{q}_{recoalescence}$:

$$\frac{\partial R_{GS}}{\partial t} \propto \dot{q}_{release} - \dot{q}_{recoalescence} \tag{4}$$

Assuming that the particles presence is most prone to amplify the turbulent intensity (Gore and Crowe, 1989) – effect (B) – then the shear stress near the elongated bubble tail increases. Since the rate of release of dispersed bubbles is directly proportional to the shear stress at the elongated bubble tail, $\dot{q}_{release} \propto \tau$, then the presence of the particles will probably increase the amount of gas dispersed bubbles in the slug body – which corroborates with the aforementioned result of Figure 5.

On the other hand, the rate of recoalescence of dispersed bubbles with the elongated bubble tail is inversely proportional to the gas-liquid interfacial tension, $\dot{q}_{recoalescence} \propto \sigma_i^{-1}$. Assuming that the particles presence increase the interfacial tension – effect (A) – then the recoalescence rate will decrease and the amount of gas in the slug body will increase. We reinforce the fact that measurements of the interfacial tension in the presence of the particles should be made in future studies, since maybe the concentration used in the experiments and the size of the particles may not influence the interfacial tension. The recoalescence rate may also be disturbed due to the particles presence not only in the liquid-gas interface, but in the liquid continuous phase between the dispersed bubbles and the elongated bubble tail. Further investigations are required to understand if those mechanisms are actually playing a role on the amount of dispersed bubbles in the slug body in the presence of solid particles.

5. CONCLUSIONS

Three-phase solid-water-air slug flow was experimentally measured, for the first time, using hydrate-like particles (polyethylene, 938 kg/m^3, 0.5 mm diameter) in a horizontal 26-mm ID pipe and compared to water-air slug flows at the same conditions to show the influence of the introduction of the solid particles on the slug flow hydrodynamics. From the flow visualization, the elongated bubble nose morphology does not appear to change with the introduction of the solid particles. The film region and the slug body appear to be more aerated in the presence of the particles, possible due to: (i) higher shear stresses since the particles used are most prone to amplify the turbulence intensity and (ii) lower coalescence rates due to variations in the interfacial tension. Those evidences are yet to be studied in future studies (e.g., measurement of size and distribution of the dispersed bubbles in the film and slug regions, measurement of the interfacial tension in the presence of the used particles).

6. ACKNOWLEDGEMENTS

The authors acknowledge the financial support of ANP and FINEP through the Human Resources Program for Oil and Gas Segment PRH-ANP (PRH 10-UTFPR), TE/CENPES/PETROBRAS (0050.0068718.11.9) and the National Council for Scientific and Technological Development (CNPq). AKS thanks PETROBRAS for sponsoring his sabbatical leave at UTFPR during the time part of this study was performed.

7. REFERENCES

Bassani, C.L., Pereira, F.H.G., Barbuto, F.A.A., Morales, R.E.M., 2016. Modeling the scooping phenomenon for the heat transfer in liquid-gas horizontal slug flows. Appl. Therm. Eng. 98, 862–871. doi:10.1016/j.applthermaleng.2015.12.104

Camargo, R.M.T., Palermo, T., Sinquin, A., Glenat, P., 2000. Rheological Characterization of Hydrate Suspensions in Oil Dominated Systems. Ann. N. Y. Acad. Sci. 912, 906–916. doi:doi:10.1111/j.1749-6632.2000.tb06844.x

Cardoso, C.A.B.R., Gonçalves, M.A.L., Camargo, R.M.T., 2015. Design options for avoiding hydrates in deep offshore production. J. Chem. Eng. Data 60, 330–335. doi:dx.doi.org/10.1021/je500601f

Castillo, F.V., 2013. An Experimental Characterization of Intermittent Two-Phase Gas-Liquid Flows in Horizontal Pipes (in Portuguese). Master Thesis, Federal University of Technology – Paraná, Curitiba/Brazil, 138 p.

Crowe, C.T., Schwarzkopf, J.D., Sommerfeld, M., Tsuji, Y., 2012. Multiphase Flows with Droplets and Particles, 2nd ed Taylor & Francis Group, Boca Raton/USA.

Dabirian, R., Mohan, R., Shoham, O., 2016a. Solid-Particles Flow Regimes in Air/Water Stratified Flow in a Horizontal Pipeline. Oil Gas Facil. 5, SPE-174960-PA. doi:10.2118/174960-PA

Dabirian, R., Mohan, R., Shoham, O., Kouba, G., 2016b. Critical sand deposition velocity for gas-liquid stratified flow in horizontal pipes. J. Nat. Gas Sci. Eng. 33, 527–537. doi:10.1016/j.jngse.2016.05.008

Doron, P., Barnea, D., 1993. A three-layer model for solid-liquid flow in horizontal pipes. Int. J. Multiph. Flow 19, 1029–1043. doi:10.1016/0301-9322(93)90076-7

Doron, P., Granica, D., Barnea, D., 1987. Slurry flow in horizontal pipes-experimental and modeling. Int. J. Multiph. Flow 13, 535–547. doi:10.1016/0301-9322(87)90020-6

Fox, R.W., Pritchard, P.J., McDonald, A.T., 2011. Fox and McDonald's Introduction to Fluid Mechanics, 8th ed. John Wiley & Sons Inc., Hoboken/USA.

França, F.A., Bannwart, A.C., Camargo, R.M.T., Gonçalves, M.A.L., 2008. Mechanistic Modeling of the Convective Heat Transfer Coefficient in Gas-Liquid Intermittent Flows. Heat Transf. Eng. 29, 984–998. doi:10.1080/01457630802241091

Goharzadeh, A., Rodgers, P., 2009. Experimental characterization of solid particle transport by slug flow using Particle Image Velocimetry. J. Phys. Conf. Ser. 147, 12069. doi:10.1088/1742-6596/147/1/012069

Goharzadeh, A., Rodgers, P., Touati, C., 2010. Influence of gas-liquid two-phase intermittent flow on hydraulic sand dune migration in horizontal pipelines. J. Fluids Eng. 132, 71301. doi:10.1115/1.4001869

Gore, R.A., Crowe, C.T., 1989. Effect of particle size on modulating turbulent intensity. Int. J. Multiph. Flow 15, 279–285. doi:10.1016/0301-9322(89)90076-1

Guer, Y. Le, Reghem, P., Petit, I., Stutz, B., 2003. Experimental study of a buoyant particle dispersion in pipe flow. Chem. Eng. Res. Des. 81, 1136–1143. doi:10.1205/026387603770866290

Issa, R.I., Kempf, M.H.W., 2003. Simulation of slug flow in horizontal and nearly horizontal pipes with the two-fluid model. Int. J. Multiph. Flow 29, 69–95. doi:10.1016/s0301-9322(02)00127-1

Kaushal, D.R., Sato, K., Toyota, T., Funatsu, K., Tomita, Y., 2005. Effect of particle size distribution on pressure drop and concentration profile in pipeline flow of highly concentrated slurry. Int. J. Multiph. Flow 31, 809–823. doi:10.1016/j.ijmultiphaseflow.2005.03.003

Kaushal, D.R., Tomita, Y., 2002. Solids concentration profiles and pressure drop in pipeline flow of multisized particulate slurries. Int. J. Multiph. Flow 28, 1697–1717. doi:10.1016/S0301-9322(02)00047-2

Kjeldby, T.K., Henkes, R. a W.M., Nydal, O.J., 2013. Lagrangian slug flow modeling and sensitivity on hydrodynamic slug initiation methods in a severe slugging case. Int. J. Multiph. Flow 53, 29–39. doi:10.1016/j.ijmultiphaseflow.2013.01.002

Krieger, I.M., Dougherty, T.J., 1959. A mechanism for non-newtonian flow in suspensions of rigid spheres. Trans. Soc. Rheol. 3, 137–152.

Mazza, R.A., Rosa, E.S., Yoshizawa, C.J., 2010. Analyses of liquid film models applied to horizontal and near horizontal gas-liquid slug flows. Chem. Eng. Sci. 65, 3876–3892. doi:10.1016/j.ces.2010.03.035

Orell, A., 2007. The effect of gas injection on the hydraulic transport of slurries in horizontal pipes. Chem. Eng. Sci. 62, 6659–6676. doi:10.1016/j.ces.2007.07.067

Peker, S., Helvaci, S., 2007. Solid-liquid two-phase flow, 1st ed., Elsevier Science, Amsterdam/Netherlands.

Rogero, E.C., 2009. Experimental Investigation of Developing Plug and Slug Flows. PhD Thesis, Tecnhische Universität München, Munich/Germany, 138 p.

Rohatgi, A., 2010. Web Plot Digitizer 3.9 [WWW Document]. URL http://arohatgi.info/WebPlotDigitizer (accessed 2.23.16).

Shoham, O., 2006. Mechanistic modeling of gas-liquid two-phase flow in pipes, 1st ed. Society of Petroleum Engineers, Richardson/USA.

Sloan, D., Koh, C., Sum, A.K., 2011. Natural gas hydrates in flow assurance, 1st ed. Elsevier Inc., Burlington/USA.

Sloan, E.D., Koh, C.A., 2008. Clathrate hydrates of natural gases, 3rd ed. Taylor & Francis Group, Boca Raton/USA.

Stevenson, P., Thorpe, R.B., 2003. Energy dissipation at the slug nose and the modeling of solids transport in intermittent flow. Can. J. Chem. Eng. 81, 271–278. doi:10.1002/cjce.5450810213

Stevenson, P., Thorpe, R.B., 2002. Velocity of isolated particles along a pipe in stratified gas-liquid flow. AIChE J. 48, 963–969. doi:10.1002/aic.690480506

Stevenson, P., Thorpe, R.B., Kennedy, J.E., McDermott, C., 2001. The transport of particles at low loading in near-horizontal pipes by intermittent flow. Chem. Eng. Sci. 56, 2149–2159. doi:10.1016/S0009-2509(00)00491-7

Taitel, Y., Barnea, D., 1990. A consistent approach for calculating pressure drop in inclined slug flow. Chem. Eng. Sci. 45, 1199–1206. doi:10.1016/0009-2509(90)87113-7

Taitel, Y., Dukler, A.E., 1976. A model for predicting flow regime transitions in horizontal and near horizontal gas-liquid flow. AIChE J. 22, 47–55. doi:10.1002/aic.690220105

Thaker, J., Banerjee, J., 2016. On intermittent flow characteristics of gas–liquid two-phase flow. Nucl. Eng. Des. doi:http://dx.doi.org/10.1016/j.nucengdes.2016.10.020

Wallis, G.B., 1969. One dimensional two-phase flow, 1st ed. McGraw-Hill, New York/USA.

8. RESPONSIBILITY NOTICE

The authors are the only responsible for the printed material included in this paper.